Nanoscale

PAPER

View Article Online
View Journal | View Issue

Cite this: *Nanoscale*, 2025, **17**, 11071

A fluorescent nonconjugated zwitterionic polymer dot: hydrothermal synthesis and application in the nano-molar sensing of 2,4,6-trinitrophenol†

Soumen Ghosh, Aayush Anand and Subrata Chattopadhyay *

Received 31st January 2025,
Accepted 27th March 2025

DOI: 10.1039/d5nr00455a

rsc.li/nanoscale

Developing nonconjugated polymer dot-based sensors with high quantum yield for a targeted application is a challenging research field. Herein, we report the synthesis of a zwitterionic polymer dot (PD PAMAM 2.5, average diameter 12 nm), which contains a poly(aminoamide) core and amine and acid groups on the surface. The molecular structure and functionalities of the polymer dot were carefully established using various spectroscopic techniques, including NMR, FTIR, and XPS. The polymer dot revealed greenish blue/aqua emission (λ_{max} = 470 nm) with a quantum yield of 28%. The mechanism for the synthesis of polymer dot with respect to its structure and fluorescence property was examined using a combination of techniques, including NMR, zeta potential and fluorescence spectrometry. The application of the fluorescent polymer dot for the selective detection of 2,4,6-trinitrophenol was studied in detail. The limit of detection was determined to be 0.77 nM, which was the best value among the current state-of-the-art. Furthermore, application of the polymer dot in real life scenarios was demonstrated using real life wastewater samples and a paper-based strip-test method.

Introduction

In recent years fluorescent nanomaterials, such as carbon dots,[1,2] quantum dots,[3] polymer dots,[4–6] nanoparticles,[7] microgels[8,9] and aggregation-induced emission molecules,[10,11] have been crucial to environmental and biological sciences. Among them, polymer dots have garnered significant attention owing to their diverse functionalities and excellent luminous characteristics[6,12,13] Depending on the molecular structure of the synthetic precursor molecule, polymer dots can be classified as conjugated polymer dots (CPDs) and non-conjugated polymer dots (NCPDs).

CPDs are formed from conjugated polymer networks. Owing to the presence of traditional conjugated fluorophores, conjugated polymer dots (CPDs) have excellent fluorescent properties with high fluorescence intensities, high quantum yields, multicolor fluorescence, and a clear luminescence mechanism. However, the same structural backbone results in poor water solubility and higher toxicity for practical applications, such as chemical sensing and biological analysis. Besides, the preparation of conjugated polymer dots involves multistep synthetic routes and the use of environmentally harmful organic chemicals and solvents.[14–16]

Therefore, the development of nonconjugated polymer dots (NCPDs) arises as a fascinating research topic. NCPDs are composed of non-conjugated polymeric backbones, containing various sub-fluorophores, such as double-bonded heteroatoms (C═O, C═N, and C═S) and amine groups.[12] In the literature, several polymeric backbones are reported to develop NCPDs, which include polyethyleneimine, polyvinyl alcohols, polylactic acid, polyacrylamides, polyacrylates, polyamides, and polyurea.[13,17–21] Such polymer backbones result in better water solubility, but at the same time nonconjugated polymer dots have lesser emission intensity and quantum yield. Though their rigid aggregated structure and crosslinking could improve the quantum yield (crosslinked enhanced emission) to a certain extent, the quantum yield of most of the reported nonconjugated polymer dots remains less than 15–20%.[22–24] Therefore, it is indispensable to further explore the development of NCPDs from other non-conventional fluorescent polymer backbones and improve their luminescent properties and quantum yield for specific applications.

Herein, we report the design and synthesis of a poly(aminoamide)-based zwitterionic polymer dot. Poly(aminoamide)s are an important class of nonconventional fluorescent polymers, which exhibit fluorescent emission mainly due to n–π* transition and the formation of localized clusters *via* the interactions of alternating amines and amides within the

Department of Chemistry, Indian Institute of Technology Patna, Bihta, Patna 801106, Bihar, India. E-mail: sch@iitp.ac.in

†Electronic supplementary information (ESI) available: Experimental and characterization details. See DOI: https://doi.org/10.1039/d5nr00455a

network.[25,26] In the past, fluorescent properties of such poly (aminoamide)s are well explored in the literature,[27–32] but they are never reported in the context of nanodot synthesis. In recent years, our works have described the synthesis of different temperature and pH responsive biocompatible poly (aminoamide) based microgels for different sensing applications, which include different ions and ratiometric determination of temperature and pH.[26,33,34] However, for the detection of external analytes, the limit of detection remains on the slightly higher side, which restricts their further developments. This is mainly ascribed to the low quantum yield of the poly(aminoamide) polymers and microgels (<5%). Therefore, we hypothesize that development of more structurally rigid polymer dots is probably the solution to enhance the emission intensity and quantum yield, and the presence of zwitterionic surface functionalities is definitely the key for their application in the sensing of nitro explosives.

In modern industry, nitro explosives are frequently employed in the domains of dyestuffs, insecticides, and pharmaceutical intermediates. Nitro explosives (significant raw ingredients in explosives) have also been linked to the rise in terrorist attacks that have put public safety, human health, and homeland security at risk.[35,36] Therefore, trace detection of nitro explosives (especially 2,4,6-trinitrophenol) remains a very important research topic. Currently developed approaches for determining nitro explosives include proton transfer-assisted soft chemical ionization mass spectrometry and immunosensing based on surface plasmon resonance.[37,38] One could argue that the practical applicability of the current approaches is limited as the approaches are costly, and require time-consuming steps that could be problematic to apply in the field.[39] Thus, researchers have been quite focused on developing portable, reliable, and affordable technologies for nitro explosive detection. In recent years several fluorophores are reported to detect 2,4,6-trinitrophenol, which include graphitic nanomaterials, metal nanoparticles, MOFs, polymers, carbon dots, quantum dots, *etc*.[40–45] However the limit of detection with polymer based sensors remains higher and very few of them are ever explored in real life test samples. Besides, polymer dots are rarely explored to detect nitro explosives. Only Liu *et al.* reported the use of a polyethyleneimine-based polymer dot to detect picric acid; however, the limit of detection was much higher, reported to be 0.5 μM.[46] Therefore application of suitable designed polymer dots to detect such nitro explosives is indispensable.

Results and discussion

Synthesis and characterization of the non-conjugated polymer dot (NCPD)

The polymer dot (PD PAMAM 2.5) was synthesized *via* a consecutive two step reaction between *N*,*N*′-methylene (bis) acrylamide (MBA) and tris-(2-amino ethylamine) as described in Scheme 1. The molecular structure of the polymer dot was characterized by NMR, FT-IR and XPS analysis. The core of the polymer dot is composed of a poly(aminoamide) backbone as a result of aza-Michael reaction between amine and acrylamide and their corresponding backbone peaks in ^{1}H-NMR were observed between 2 and 3.5 ppm and at 4.5 ppm (methylene peaks) (Fig. 1A). The surface groups of the zwitterionic quantum dots contain acid and amine functionalities and they are characterized *via* a combination of techniques. ^{13}C-NMR revealed the existence of two carbonyl peaks (amide and acid) at 175 and 178 ppm (Fig. 1A). Further the polymer dot structure was analyzed by FTIR spectroscopy (Fig. 1B). The formation of (–COO$^-$) is supported by the FTIR spectra where the asymmetric and symmetric stretching vibrations of carboxylates (–COO$^-$) are represented by the distinctive peaks at 1548 cm^{-1} and 1387 cm^{-1} respectively.[47] The stretching vibrations of N–H were linked to the absorption band centered at 3146 cm^{-1}. The typical band representing the asymmetric stretching of the C–N bond is noted at 1115 cm^{-1}.

To further confirm the functional groups and structure of PD PAMAM 2.5, detailed XPS analysis was conducted. Examining the XPS scanning spectra as a whole (Fig. 1C) reveals distinctive peaks of C 1s, N 1s, and O 1s at 285, 399, and 531 eV, respectively.[48] Carbon, nitrogen, and oxygen were detected by full scan XPS analysis. Further analysis of the C 1s band at 285 eV clearly revealed different characteristic peaks, two peaks representing the C–C and C–N groups observed at 283.84 eV and 285.4 eV, respectively (Fig. 1D).[49] The peak at 286.6 eV supports the formation of carboxylate ions (–COO$^-$) on the surface of the polymer dot.[50] The O═C–N (399.7 eV) peak was detected in the high-resolution N 1s spectra and the presence of surface amine is confirmed as the N–H peak can be detected in the high-resolution N 1s spectra at 398.26 eV (Fig. 1E).[51] Similar deconvolution of the O 1s signal results in two peaks at 530.2 eV and 531.83 eV (Fig. 1F), which showed the existence of C═O and C–OH, respectively.[50,51] All these combined spectroscopic analyses confirm the poly(aminoamide) core and presence of both carboxylate and amine on the surface of the polymer dot (PD PAMAM 2.5). Additionally, the presence of surface amine groups is confirmed by the ninhydrin test (Fig. S1†). Further, a broad peak is noted in the powder X-ray diffraction (PXRD) spectra, which is centered at around $2\theta = 22°$ (Fig. S2†). This peak reveals the amorphous structure with highly disordered carbon and polymer chains. No graphitic peak is present at around $2\theta = 26°$, which suggests that the NCPDs were composed of a non-graphitized architecture.[50] Additionally, the TGA thermogram (Fig. S3†) of the polymer dot reveals that the polymer dot is thermally stable at least until 200 °C, which is atypical of the thermal stability of poly(aminoamide) backbones.[52–57]

Further, the reaction is monitored at different time intervals by ^{1}H and ^{13}C NMR and zeta potential analysis to establish the mechanistic steps in the synthesis of zwitterionic polymer dot. ^{1}H NMR analysis after 30 minutes of reaction under ambient conditions (step 1 in Scheme 1) reveals small oligomeric structures, representing 50% conversion of the acrylamide groups (via the integration ratio of three different

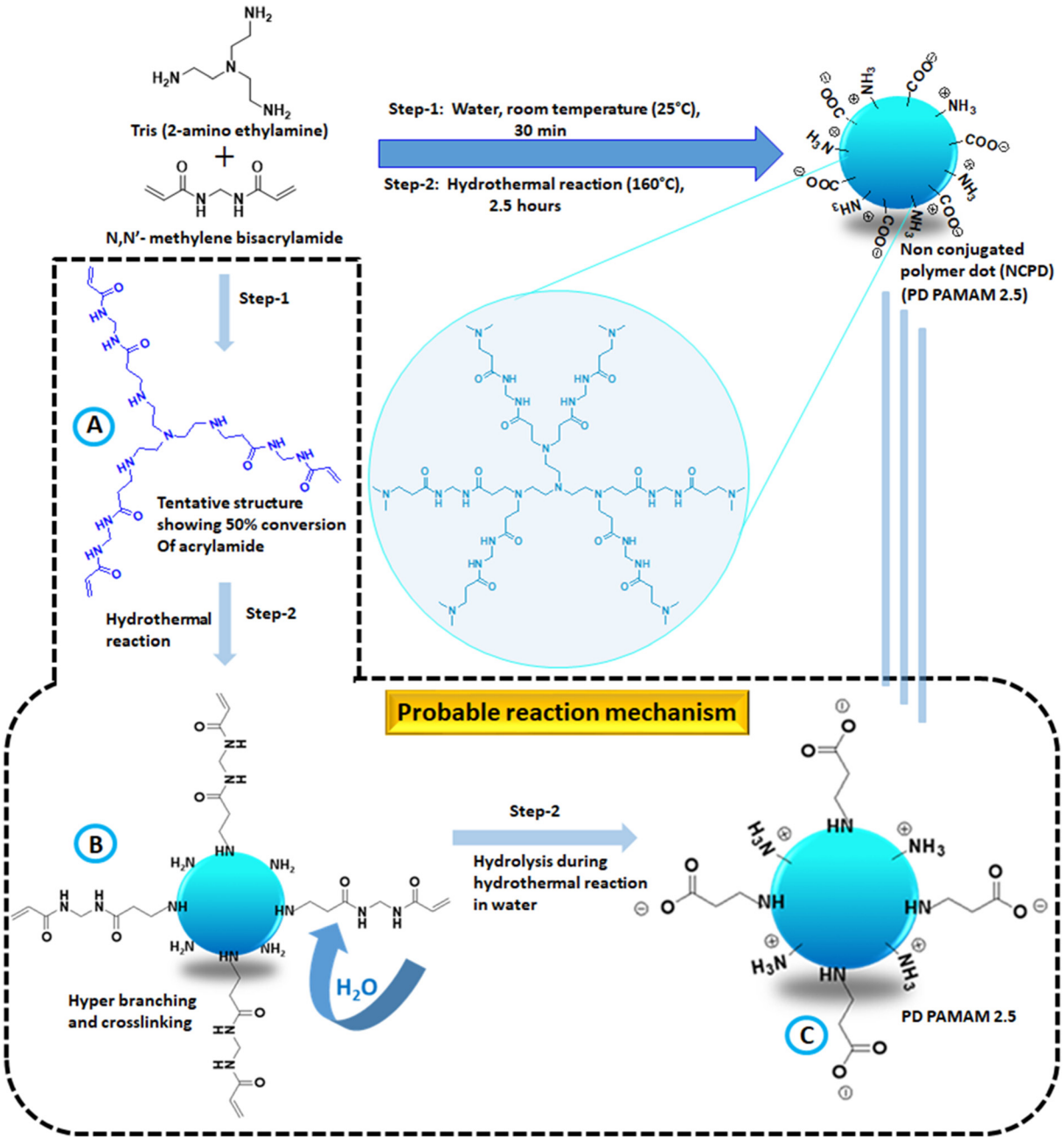

Scheme 1 Synthesis of the non-conjugated polymer dot (NCPD) PD PAMAM 2.5 and its mechanistic steps.

peaks, $I_{b+c+d} : I_a : I_{f+g+h}$, Fig. S4A†), which is expected to form a tentative tetrameric form as represented by structure A in Scheme 1. Further structures formed during the hydrothermal treatment (step 2 in Scheme 1) were also analyzed by ^{1}H and ^{13}C NMR spectra at different time intervals to support the reaction mechanism and understand the formation of different functional groups (Fig. S4†). After 30 minutes of the hydrothermal reaction, ^{1}H NMR reveals the formation of a polymeric core with surface acrylamide groups (structure B in Scheme 1). After 2 hours of the reaction, ^{1}H NMR indicates the complete disappearance of surface acryl peaks, while the core remains unchanged. This indicates the hydrolysis reaction during the process. To evidence that further, the respective ^{13}C NMR spectra are analyzed at different time intervals (Fig. S4B†). Two carbonyl carbon peaks after 2 hours of hydrothermal treatment clearly signify significant generation of acid groups on the surface (besides the existing amide groups), revealing zwitterionic surface formation (structure C in Scheme 1). Additionally, zeta potential was measured to confirm the similar appearance of negatively charged carboxylate groups on the surface. After 30 minutes and 1 hour of hydrothermal treatment, the zeta potential of the polymer dot was measured

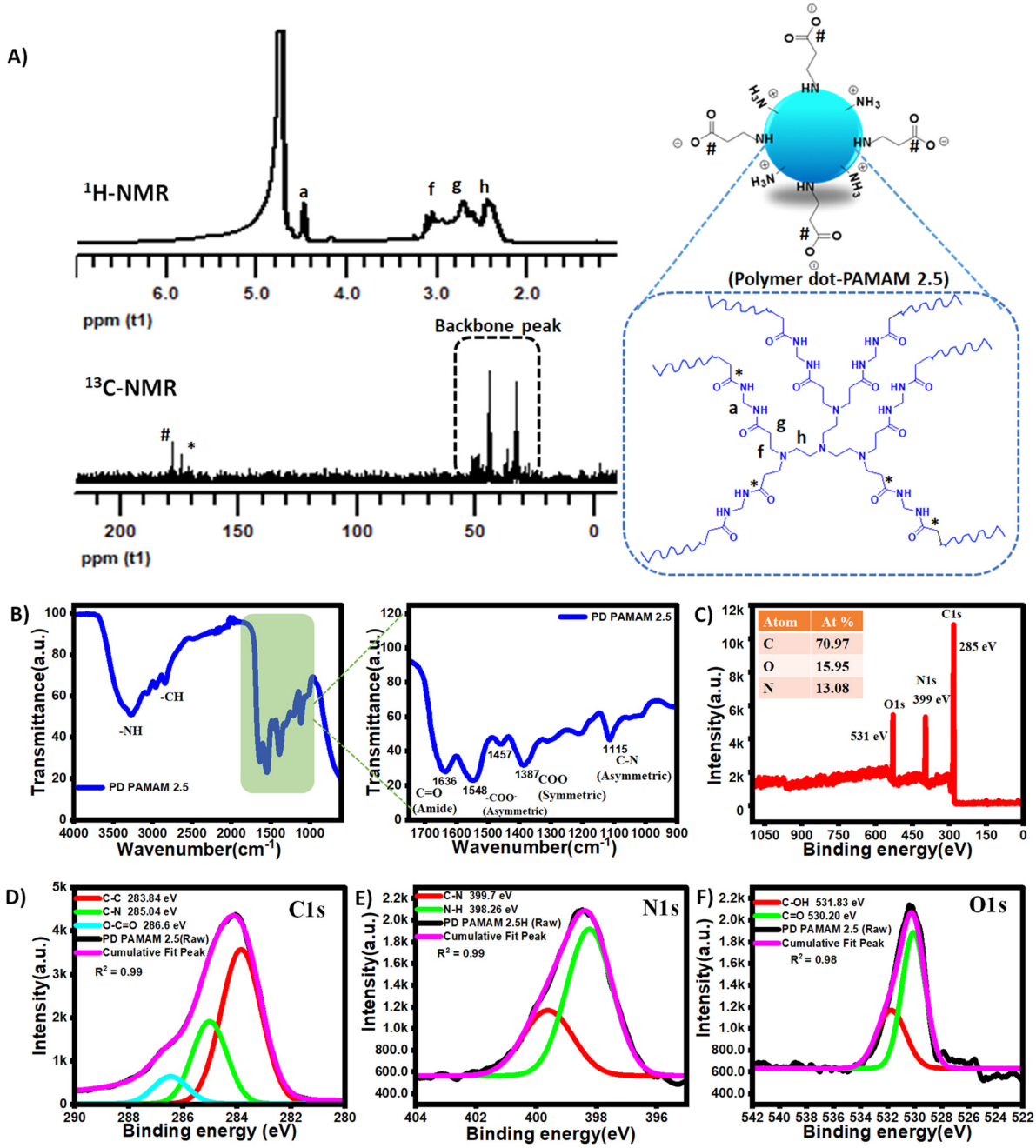

Fig. 1 Molecular characterization of the polymer dot: (A) ^{1}HNMR and ^{13}C-NMR spectra of PD PAMAM 2.5. (B) FTIR spectra of PD PAMAM 2.5. (C) Full scan XPS survey spectra of PD PAMAM 2.5. XPS spectra with high resolution of (D) C 1s, (E) O 1s, and (F) N 1s.

to be 17–18 mV (indicating the presence of positively charged amine groups predominantly) (Fig. S5 and Table S1†), while the zeta potential sharply drops to lower than 5 mV after 2 hours of hydrothermal reactions – supporting again the generation of significant negatively charged carboxylate groups, in addition to the existing amine groups on the surface, which consecutively supports the reaction mechanism, as described in Scheme 1.

The size and shape of the polymer dot was characterized using DLS, TEM and AFM. The DLS CONTIN plot indicates that the average diameter of the polymer dot was ~12 nm (Fig. 2A). The TEM micrograph revealed an average size of the polymer dot as 8–10 nm (Fig. 2B). Additionally, atomic force microscopy (AFM) micrographs also supported the same (Fig. 2C). However, the size of the polymer dot as revealed in the AFM micrograph was ~20 nm. The slightly higher size in the AFM micrograph is due to the softer nature of the polymer dot, which flattened when coated on a silicon surface, which is also supported *via* height profile analysis and a 3D image (Fig. 2D and Fig. S6†).

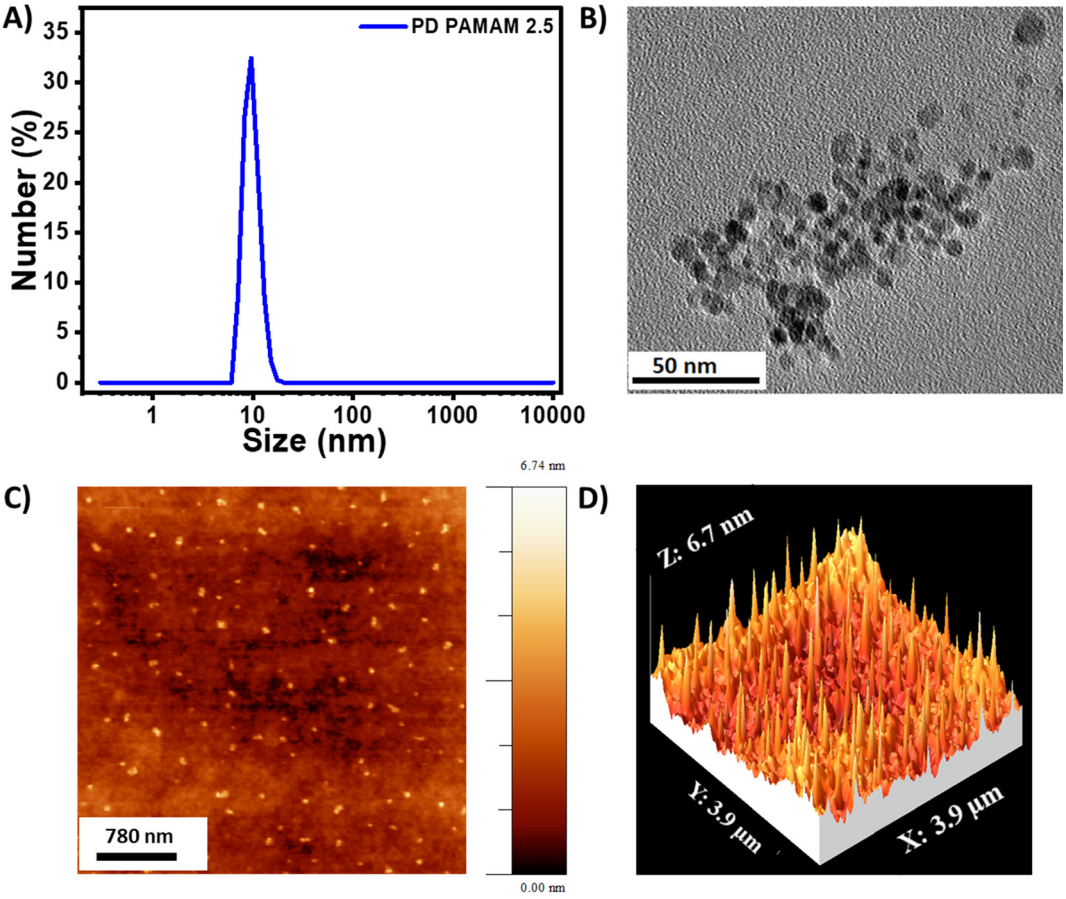

Fig. 2 (A) Hydrodynamic diameter of PD PAMAM 2.5, (B) TEM micrograph of PD PAMAM 2.5, (C) AFM micrograph of PD PAMAM 2.5, and (D) 3D AFM image of PD PAMAM 2.5.

Fluorescent properties of the polymer dot

Absorption and fluorescence spectroscopies were used to examine the photophysical characteristics of the polymer dot (PD PAMAM 2.5). The absorption and excitation/emission spectra of PD PAMAM 2.5 are shown in Fig. 3. The PD PAMAM 2.5 exhibits an overlap between their absorption band peak at 365 nm and excitation band peak at 350 nm (Fig. 3). When exited at 350 nm, PD PAMAM 2.5 shows the highest fluorescence intensity at 470 nm (appearing as aqua/greenish blue). Further, the quantum yield of the polymer dot was determined with respect to quinine sulfate and reported to be

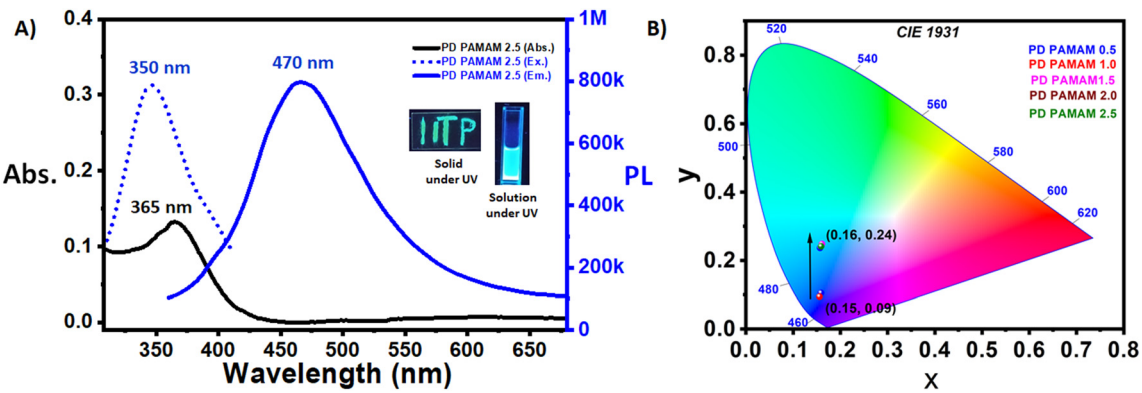

Fig. 3 (A) Absorption spectra of PD PAMAM 2.5, and the fluorescence excitation/emission spectra of PD PAMAM 2.5 (the inset image displays the solid and aq. solution states of PD PAMAM 2.5 under UV light (λ_{ex} = 365 nm)). (B) CIE 1931 chromaticity diagram of the polymer dot and its variations at different stages of synthesis (λ_{ex} = 350 nm).

28.0%. This is surely among one of the highest quantum yields reported for nonconjugated polymer dots and best among poly(aminoamide)-based fluorescent materials, which is mainly conferred by the more structurally rigid polymer dot formation.

In general, poly(amino-amide) based hyperbranched polymers exhibit blue fluorescence at ~410–450 nm.[26,58] However, the emission spectra of the current polymer dot exhibit a λ_{max} = 470 nm (greenish blue/aqua), revealing a clear red shift. This was studied further by measuring the emission spectra of the polymer dots formed at different time intervals of the hydrothermal process. The overall details are presented in Fig. 3B and Fig. S7.† The emission spectra of polymer dots formed after 0.5 and 1 hour of hydrothermal treatment (containing acrylamide functional moieties on the surface, Scheme 1) present a λ_{max} = 410–420 nm, characteristic of poly(aminoamide) networks. However, after 2 and 2.5 hours of hydrothermal treatment (containing acid and amide groups on the surface, Scheme 1) the emission spectra of the polymer dot present a λ_{max} = 470 nm, revealing a clear red shift. The CIE 1931 chromaticity diagram exhibits a clear colour change from blue to greenish blue/aqua with the changing co-ordinates from (0.15, 0.09) to (0.16, 0.24) (Fig. 3B). Therefore, it can be noted that the red shift and greenish blue fluorescent emission of the current poly(aminoamide) structure are a result of the formation of rigid polymer dots, and presence of amine and acid surface functionalities.[59] Additionally the fluorescence intensity of the PD PAMAM 2.5 is dependent on the concentration; with increasing concentration its intensity increases as shown in Fig. S8,† due to aggregation induced emission. Further excitation dependent emission of the current polymer dot is studied (Fig. S9†). When the excitation wavelength is changed from 340 nm to 430 nm, the λ_{max} of emission spectra remains nearly unchanged, while the intensity of the fluorescent peaks decreases continuously as the excitation wavelength is increased.

Application of the polymer dot for selective detection of 2,4,6-trinitrophenol (PA)

The use of the fluorescent polymer dots in the sensing of nitro explosives is examined in detail. Fig. 4A represents the screening test in the presence of a range of nitro-aromatic compounds, which include 2,4,6-trinitrophenol (PA), 4-nitrophenol (4-NP), 2-nitrophenol (2-NP), 3-nitrophenol (3-NP), dinitrobenzene (DNB), nitrobenzene (NB), 5-nitroisophthalic acid (5-NIPA), and 5-nitroterephthalic acid (5-NTA), some other organic analytes such as benzoic acid (BA), terephthalic acid (TA), phenol (PHEN), 5-aminoisophthalic acid (5-AIPA), 2-aminophenol (2-AP), toluene (TOL), aniline (AN), and toluidine (TOLN), and aliphatic amines such as ethyl amine (EA), diethyl amine (DEA), and triethyl amine (TEA). The chemical structure of all the analytes is shown in Fig. S10.† From Fig. 4A, it is evident that, among the aromatic compounds, 2,4,6-trinitrophenol (PA) and 4-nitrophenol induce significant and selective fluorescence quenching, while their equivalents have far lower quenching efficiencies. For PA near quantitative quenching (~99%) was noted. Therefore, further detailed experiments are performed to understand the uses of the polymer dot for the sensing of PA. The interference test was performed by analyzing the fluorescence emission spectra of PD PAMAM 2.5 in the presence of only PA and the presence of both potential interfering analytes and PA, as shown in Fig. 4B and Fig. S11.† For this, the interference by the other nitro aromatic compounds and also other organic analytes on the fluorescence sensing of 2,4,6-trinitrophenol (PA) by PD PAMAM 2.5 was studied using fifteen other organic analytes (25 μM) such as 2-NP, 3-NP, DNP, NB, 5-NIPA, 5-NTA, BA, TA, PHEN, 5-AIPA, 2-AP, TOL, AN, TOLN, *etc*. and 25 μM 2,4,6-trinitrophenol (PA). The results clearly demonstrate that 2,4,6-trinitrophenol (PA)-induced fluorescence quenching of PD PAMAM 2.5 is very selective as other nitro aromatic and organic analytes do not interfere significantly.

To assess the quenching efficiency, the quenching coefficient (K_{SV}) was calculated using the Stern–Volmer equation:

$$I_0/I = 1 + K_{SV}[Q] \quad (1)$$

where I_0 is the maximum fluorescence intensity of PD PAMAM 2.5 solution, I is the intensity of PD PAMAM 2.5 solution in the presence of 2,4,6-trinitrophenol (PA), and [Q] is the concentration. 2,4,6-Trinitrophenol (PA) quenches the fluorescence of PD PAMAM 2.5 having excellent linearity between 1.24×10^{-6} M and 12.19×10^{-6} M, which corresponds to the correlation coefficient (R^2 = 0.99) and K_{SV} (3.515×10^4 M^{-1}), indicating that the solution of PD PAMAM 2.5 has higher selectivity for 2,4,6-trinitrophenol (PA). This is due to the presence of a nitro groups at the ortho and para position, which makes the aromatic ring more electron deficient and activate the –OH group to interact with the carboxylate moieties ($-COO^-$) of PD PAMAM 2.5. Utilizing the formula LOD = $3\delta/k$, where δ is the standard deviation and k is the slope derived from the intensity *vs.* concentration plot, the calculated limit of detection (LOD) was 0.77 nM (Fig. S12†). This is surely one of the lowest LOD for the selective detection of 2,4,6-trinitrophenol among various reported nanosensors (Table S2†).

Fluorescence quenching mechanism of polymer dot in the presence of 2,4,6-trinitrophenol

In the literature selective quenching by a particular analyte is explained by different mechanisms, such as dynamic quenching, static quenching, and competitive absorption.[26,60,61] The strong interaction between the fluorophore and quencher, along with the development of a nonfluorescent ground-state complex, is the usual cause of static quenching, which is expected to be the major reason in the current case due to the expected more selective interaction of zwitterionic polymer dot with PA.[62] Further multiple experiments were performed to confirm static quenching as the major quenching process for the current sensing as follows:

The process of static quenching was verified using the fluorescence lifetime decay curves of PD PAMAM 2.5 in the absence and presence of PA, as presented in Fig. 5B. Based on

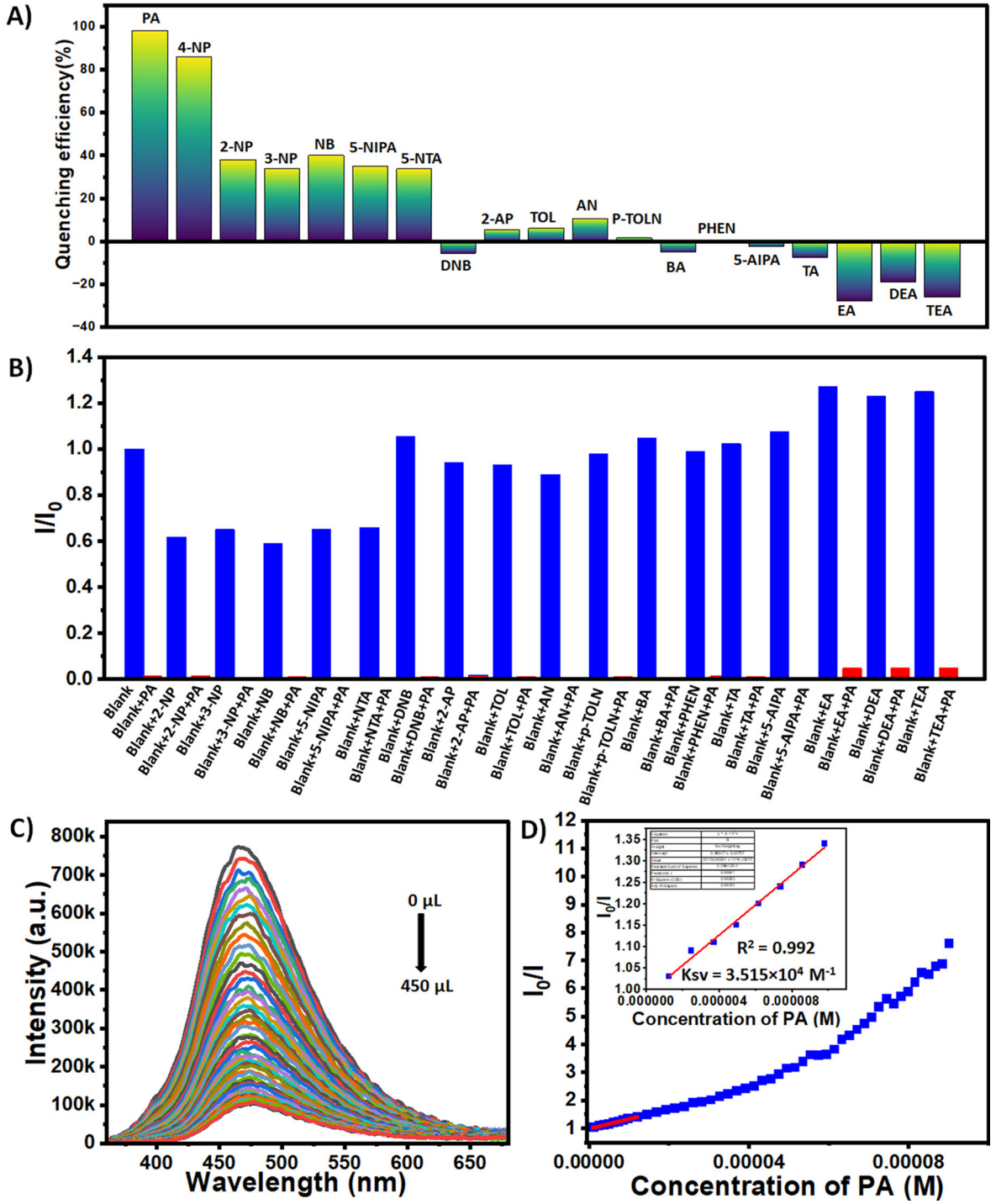

Fig. 4 (A) Quenching efficiency of the analytes for PD PAMAM 2.5, (B) fluorescence responses of the PD PAMAM 2.5 in the presence of 25 μM of other organic analytes and 25 μM of 2,4,6-trinitrophenol (PA), (C) fluorescence emission spectra of PD PAMAM 2.5 (0.15 mg ml^{-1}) in the presence of 2,4,6-trinitrophenol (PA) (0.0005 M) with excitation at 350 nm and slit width of 1.5, and (D) Stern–Volmer plot of PD PAMAM 2.5 in the presence of 2,4,6-trinitrophenol (PA).

the decay parameter, the average lifetimes of PD PAMAM 2.5 in the absence and presence of PA were calculated (Table S3†). The average fluorescence lifetime of PD PAMAM 2.5 is calculated to be 6.48 ns. Addition of PA further does not change the lifetime (calculated to be 6.44 ns when the concentration of PA is 25 μM, and 6.38 ns when the concentration of PA is even increased to 100 μM). The near constant average fluorescence lifetime of PD PAMAM 2.5 in the absence or presence of PA supports the static quenching mechanism and suggests the formation of a ground-state complex between PD PAMAM 2.5

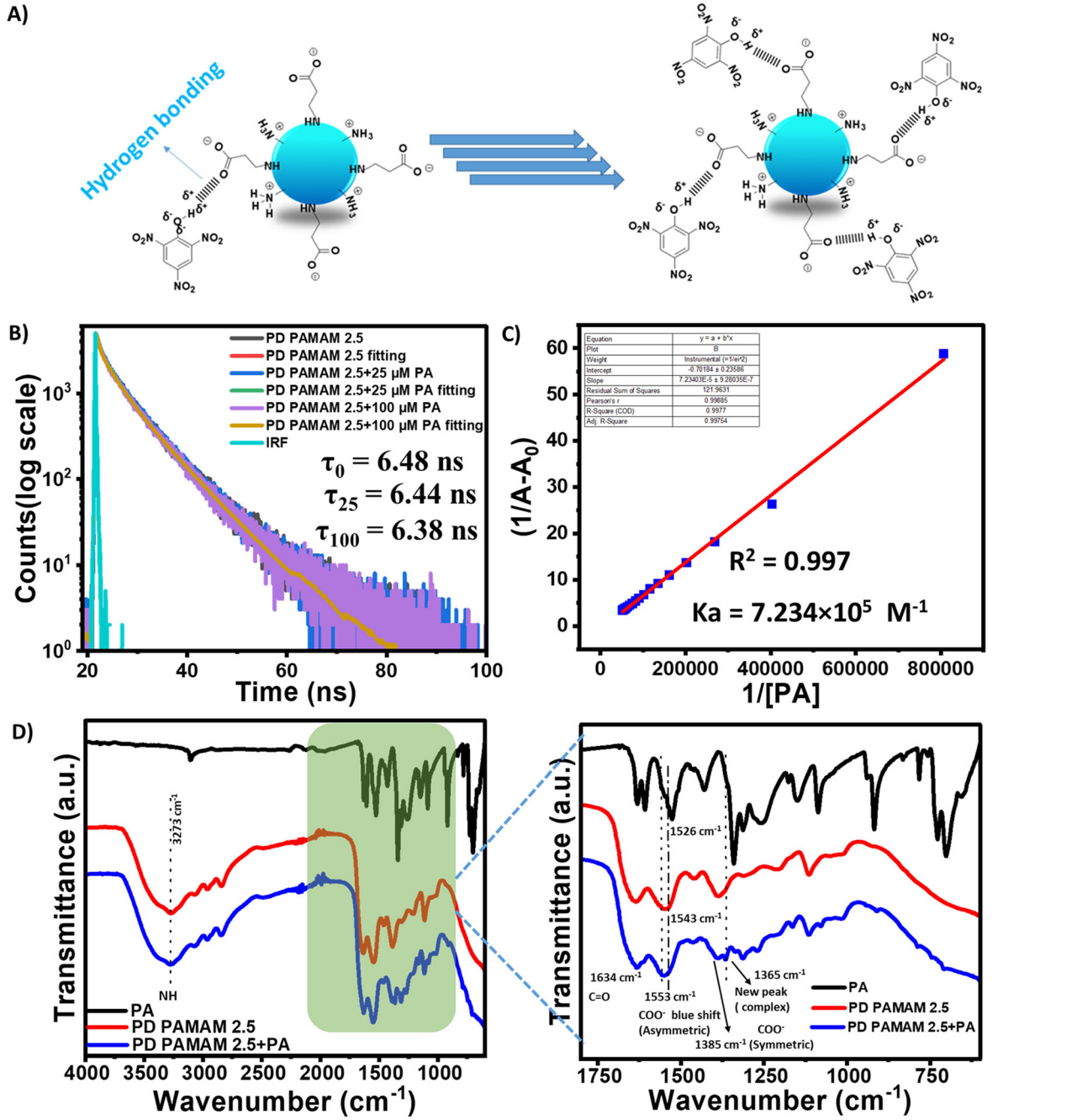

Fig. 5 (A) Plausible mechanism of interactions with PA, resulting in fluorescence quenching, (B) fluorescence decay of the PD PAMAM 2.5 in the absence and presence of 25 μM and 100 μM of 2,4,6-trinitrophenol (PA). (C) Benesi–Hildebrand plot of PD PAMAM 2.5 (0.15 mg ml^{-1}) in the presence of 2,4,6-trinitrophenol (PA) (10 mM). (D) FTIR spectra of PA, PD PAMAM 2.5 and PD PAMAM 2.5 in the presence of 2,4,6-trinitrophenol (PA) with the magnified image showing the lower wavenumber region.

and PA. Furthermore, the static quenching mechanism is supported by the Stern–Volmer curve, as shown in Fig. 4D, which does not follow a linear curve throughout. The Benesi–Hildebrand plot shown in Fig. 5C provides additional evidence that supports the static quenching mechanism. The correlation coefficient value is R^2 = 0.997 and the association constant (K_a) is derived from the linear interaction which was observed to be 7.234 × 10^5 M^{-1} between PD PAMAM 2.5 and PA (by analyzing the UV-VIS spectroscopy of PD PAMAM 2.5 in the presence and absence of PA, Fig. S13†). The creation of a robust complex between the guest (PA) and host (PD PAMAM 2.5) molecules through H-bonding is confirmed by this value.

Further to have a direct spectroscopic evidence and clarify the ground-state complex formation between PD PAMAM 2.5

and PA, the FTIR spectra (Fig. 5D) of PD PAMAM 2.5 both in the presence and absence of PA were studied. It is noted that a new peak arises at 1365 cm^{-1} along with the blue shift of the COO^- (asymmetric) peak, which is visible at 1553 cm^{-1} and shifted from 1543 cm^{-1} in the presence of PA, which supports the formation of a ground state complex *via* hydrogen bonding interaction.

Besides static quenching, other types of quenching mechanisms such as fluorescence resonance energy transfer (FRET) and inner filter effect (IFE) are also established in the literature for sensing of PA. A spectral overap between the absorption spectra of PA and excitation and emission spectra of polymer dot indicates that IFE and FRET might interfere with the static quenching process. However, it is important to note that FRET is a dynamic quenching process. Therefore, consistent fluorescence lifetime of the polymer dot in the presence and absence of PA (Fig. 5B) clearly indicated the absence of the FRET mechanism. Further to reaffirm this, spectral overlap integral values between PA (abs) and PD PAMAM 2.5 (Em) are calculated using an established process,[63,64] which clearly revealed the absence of significant FRET (Fig. S14†). In addition, the spectral overlap between the absorption spectra of PA and the excitation spectra of PD PAMAM 2.5 reveals the possibility of quenching through IFE and in this regard, we calculated the percentage of quenching by IFE using the Parker equation as established in the literature.[65,66] The detailed calculation is tabulated in Table S4.† The results revealed that IFE contributed less than 10% of overall quenching when the concentration of PA was less than 7 μM. Even at a much higher concentration of PA (19 μM) the contribution of IFE is only 22%, clearly confirming that static quenching is the major quenching mechanism for the sensing of PA.

Detection and quantification in real life water samples and test papers

To further validate the real life applicability of the PD PAMAM 2.5, further studies were performed to detect 2,4,6-trinitrophenol (PA) in both real life water samples and test paper. Three water samples were collected, which are STP water (industrial wastewater from a local sewage treatment plant in Patna, Bihar), lake water (from Begusarai, Bihar) and river water (from Ganges River, Patna, Bihar). Before the use of these water samples, we have filtered (to remove larger particles/muds, *etc.*) the water and centrifuged it for 30 min at 12 000 rpm. As the PL sensor could not detect any 2,4,6-trinitrophenol (PA) in the water samples, the samples were spiked with 2,4,6-trinitrophenol (PA) at 20 μM concentration level to perform a recovery test and validate the use of the polymer dot and quantify the level of PA using a standard curve. The findings are summarized in Table 1. There was good agreement between the added amounts and found values, and the obtained recoveries varied from 90% to 96%, indicating that these samples had no significant interferences. Furthermore, the relative standard deviations (RSD) of three replication determinations for each sample were between 0 and 3%, indicating excellent reproducibility and precision. As a result, it was anticipated that the PD PAMAM 2.5-based PL sensor could be successfully used to detect 2,4,6-trinitrophenol (PA) in real life water samples.

Table 1 Detection of spiked TNP in real life water samples (n = 3)

Water	Added (μM)	Mean found (μM)	Mean recovery[a] (%)	RSD (%)
STP water	20	19.2	96	1.73
Lake water	20	18.5	92	0.32
River water	20	18.0	90	2.02

[a] $\text{Recovery}\,(\%) = 100 \times \frac{C_{\text{mean-found}}}{C_{\text{added}}}$.

Further, a basic test paper assay is performed to validate its future use as a cheap sensor (Fig. 6). For test paper tests, a piece of paper was immersed in a sealed glass petri dish containing 10 mg mL^{-1} of polymer dot solution in water for 1 hour. Following that, the paper was taken from the solution and heated in an oven at a constant temperature of 60 °C for 1 hour to dry completely, which resulted in a polymer dot coated aqua fluorescent paper strip. Four different concentration doses (varying between 5 nM and 5 μM) of 2,4,6-trinitrophenol (PA) solution, such as 0.005 μM or 5 nM, 0.05 μM or 50 nM, 0.5 μM or 500 nM and 5 μM, were dripped onto distinct zones of the PD PAMAM 2.5-treated test paper. The prepared paper strip was dried for 2 hours at 60 °C before checking it under UV light. Under 365 nm UV light irradiation, the PL intensity of the four zones varied dramatically, and the intensity decreased as the 2,4,6-trinitrophenol (PA) concentration increased as noted in Fig. 6. The aforesaid findings suggested that a paper-based PL sensor for detecting 2,4,6-trinitrophenol (PA) within a wide concentration range is possible to be successfully manufactured in future. The paper sensor can be used with fingerprint lifting or imaging techniques to detect 2,4,6-trinitrophenol (PA) in homeland security and public safety applications.

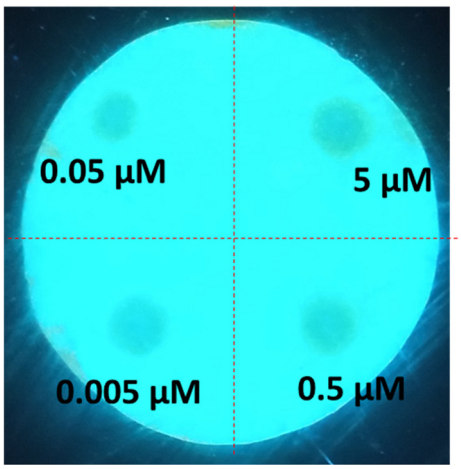

Fig. 6 Test paper assay for the detection of 2,4,6-trinitrophenol (PA). The pattern presents the concentration of 2,4,6-trinitrophenol (PA), such as 5 μM, 0.5 μM, 0.05 μM, and 0.0005 μM or 5 nM. The photo was taken under UV light (365 nm).

Conclusion

To summarize, we have successfully demonstrated the synthesis of a fluorescent zwitterionic nonconjugated polymer dot *via* a simple hydrothermal process, where both aza-Michael and hydrolysis reactions play a pivotal role in dictating the molecular structure and surface functionalities. The generation of both amine and acid functionalities on the surface was proven by a number of characterization techniques including NMR, FT-IR, XPS, zeta potential and others. The polymer dot exhibited greenish-blue emission with an excellent quantum yield of 28%. The application of the polymer dot to detect 2,4,6-trinitrophenol/picric acid (PA) was studied in detail. The LOD value was reported to be 0.77 nM for the detection of picric acid (PA). The mechanism of fluorescent quenching was established with proper evidence. We have also studied the real life applicability of the polymer dot as a nanosensor in different types of water samples, which include industrial wastewater (STP), lake water and river water, and we obtained more than 90% mean recovery with an excellent relative standard deviation less than 3%. Furthermore, basic test paper assay results clearly revealed that the polymer dot can be easily implemented to fabricate paper-based PL sensors for remote and cost-effective detection of PA in future for practical commercial applications.

Author contributions

SG: design of experiments, synthesis, characterization, application, relevant data analysis, (lead), writing (lead), AA: characterization (supporting) SC: conceptualization of the actual work and supervision, writing (lead and review). All the authors have approved the final version of the manuscript.

Data availability

The data supporting this article have been included as part of the ESI.†

Conflicts of interest

There are no conflicts to declare.

Acknowledgements

SG and AA acknowledge IITP for the research fellowship. Sophisticated Analytical Instrument Facility (SAIF) at IIT Patna is acknowledged for the DLS, TGA and zeta potential analysis, and Sprint testing solution is acknowledged for the XPS analysis with payment.

References

1 L. Đorđević, F. Arcudi, M. Cacioppo and M. Prato, *Nat. Nanotechnol.*, 2022, **17**, 112–130.
2 R. B. González-González, A. Sharma, R. Parra-Saldívar, R. A. Ramirez-Mendoza, M. Bilal and H. M. Iqbal, *J. Hazard. Mater.*, 2022, **423**, 127145.
3 D. Peng, L. Zhang, F.-F. Li, W.-R. Cui, R.-P. Liang and J.-D. Qiu, *ACS Appl. Mater. Interfaces*, 2018, **10**, 7315–7323.
4 X. Zhou, Q. Liu, W. Yuan, Z. Li, Y. Xu, W. Feng, C. Xu and F. Li, *Adv. Sci.*, 2021, **8**, 2000441.
5 Y.-T. Gao, B.-B. Chen, L. Jiang, J. Lv, S. Chang, Y. Wang, R.-C. Qian, D.-W. Li and M. E. Hafez, *ACS Appl. Mater. Interfaces*, 2021, **13**, 50228–50235.
6 H. Zhang, X. Dong, J. Wang, R. Guan, D. Cao and Q. Chen, *ACS Appl. Mater. Interfaces*, 2019, **11**, 32489–32499.
7 R. Santonocito, M. Intravaia, I. M. Caruso, A. Pappalardo, G. T. Sfrazzetto and N. Tuccitto, *Nanoscale Adv.*, 2022, **4**, 1926–1948.
8 S. Kumari, M. Avais and S. Chattopadhyay, *ACS Appl. Polym. Mater.*, 2023, **5**, 1626–1645.
9 M. Arif, *J. Environ. Chem. Eng.*, 2023, **11**, 109270.
10 X. Zhang, K. Wang, M. Liu, X. Zhang, L. Tao, Y. Chen and Y. Wei, *Nanoscale*, 2015, **7**, 11486–11508.
11 M. H. Chua, K. L. O. Chin, X. J. Loh, Q. Zhu and J. Xu, *ACS Nano*, 2023, **17**, 1845–1878.
12 S. Zhu, Y. Song, J. Shao, X. Zhao and B. Yang, *Angew. Chem., Int. Ed.*, 2015, **54**, 14626–14637.
13 S. G. Liu, T. Liu, N. Li, S. Geng, J. L. Lei, N. B. Li and H. Q. Luo, *J. Phys. Chem. C*, 2017, **121**, 6874–6883.
14 D. Kim and T. S. Lee, *ACS Appl. Mater. Interfaces*, 2016, **8**, 34770–34776.
15 J. Kim and T. S. Lee, *Macromol. Rapid Commun.*, 2016, **37**, 303–310.
16 E. Woźnica, K. Maksymiuk and A. Michalska, *Anal. Chem.*, 2014, **86**, 411–418.
17 Y. Wang, A. Warshawsky, C. Wang, N. Kahana, C. Chevallard and V. Steinberg, *Macromol. Chem. Phys.*, 2002, **203**, 1833–1843.
18 S. Zhang, T. Liu, B. Zhao, C. Verdi, W. Liu, C. Hao and J. Zhang, *Polymer*, 2020, **209**, 122980.
19 J. Wang, L. Xu, S. Zhong, Y. Yang, G. Feng, Q. Meng, Y. Gao and X. Cui, *Polym. Chem.*, 2021, **12**, 7048–7055.
20 L. Vallan, E. P. Urriolabeitia, F. Ruipérez, J. M. Matxain, R. Canton-Vitoria, N. Tagmatarchis, A. M. Benito and W. K. Maser, *J. Am. Chem. Soc.*, 2018, **140**, 12862–12869.
21 S. Kumari, M. Avais and S. Chattopadhyay, *Polymer*, 2022, **256**, 125219.
22 Y. Chen, Y. Zhang, T. Lyu, Y. Wang, X. Yang and X. Wu, *J. Mater. Chem. C*, 2019, **7**, 9241–9247.
23 L. Vallan, E. P. Urriolabeitia, A. M. Benito and W. K. Maser, *Polymer*, 2019, **177**, 97–101.
24 S. G. Mucha, L. Firlej, J.-L. Bantignies, A. Żak, M. Samoć and K. Matczyszyn, *RSC Adv.*, 2020, **10**, 38437–38445.
25 R.-B. Wang, W.-Z. Yuan and X.-Y. Zhu, *Chin. J. Polym. Sci.*, 2015, **33**, 680–687.

26 S. Ghosh, M. Avais and S. Chattopadhyay, *Chem. Commun.*, 2022, **58**, 12807–12810.
27 W. Yang and C. Y. Pan, *Macromol. Rapid Commun.*, 2009, **30**, 2096–2101.
28 Y.-J. Tsai, C.-C. Hu, C.-C. Chu and T. Imae, *Biomacromolecules*, 2011, **12**, 4283–4290.
29 G. Wang, L. Fu, A. Walker, X. Chen, D. B. Lovejoy, M. Hao, A. Lee, R. Chung, H. Rizos and M. Irvine, *Biomacromolecules*, 2019, **20**, 2148–2158.
30 C. Zhan, X.-B. Fu, Y. Yao, H.-J. Liu and Y. Chen, *RSC Adv.*, 2017, **7**, 5863–5871.
31 W. I. Lee, Y. Bae and A. J. Bard, *J. Am. Chem. Soc.*, 2004, **126**, 8358–8359.
32 D. Wang and T. Imae, *J. Am. Chem. Soc.*, 2004, **126**, 13204–13205.
33 S. Ghosh, J. D. Katiyar and S. Chattopadhyay, *Soft Matter*, 2024, **20**, 79–88.
34 S. Ghosh, A. Anand and S. Chattopadhyay, *J. Appl. Polym. Sci.*, 2024, e56614.
35 A. Rose, Z. Zhu, C. F. Madigan, T. M. Swager and V. Bulović, *Nature*, 2005, **434**, 876–879.
36 J. Huang, J. Gu, Z. Meng, X. Jia and K. Xi, *Nanoscale*, 2015, **7**, 15413–15420.
37 D. R. Shankaran, K. V. Gobi, K. Matsumoto, T. Imato, K. Toko and N. Miura, *Sens. Actuators, B*, 2004, **100**, 450–454.
38 B. Agarwal, R. N. González-Méndez, M. Lanza, P. Sulzer, T. D. Märk, N. Thomas and C. A. Mayhew, *J. Phys. Chem. A*, 2014, **118**, 8229–8236.
39 K. Bauri, B. Saha, J. Mahanti and P. De, *Polym. Chem.*, 2017, **8**, 7180–7187.
40 Y. Zou, K. Huang, X. Zhang, D. Qin and B. Zhao, *Inorg. Chem.*, 2021, **60**, 11222–11230.
41 B. Qu, Z. Mu, Y. Liu, Y. Liu, R. Yan, J. Sun, Z. Zhang, P. Li and L. Jing, *Environ. Sci. Nano*, 2020, **7**, 262–271.
42 O. M. K. Koç, A. Uzer and R. A. Apak, *ACS Appl. Mater. Interfaces*, 2023, **15**, 42066–42079.
43 B. B. Chen, Z. X. Liu, H. Y. Zou and C. Z. Huang, *Analyst*, 2016, **141**, 2676–2681.
44 D. Peng, L. Zhang, F.-F. Li, W.-R. Cui, R.-P. Liang and J.-D. Qiu, *ACS Appl. Mater. Interfaces*, 2018, **10**, 7315–7323.
45 S. G. Liu, D. Luo, N. Li, W. Zhang, J. L. Lei, N. B. Li and H. Q. Luo, *ACS Appl. Mater. Interfaces*, 2016, **8**, 21700–21709.
46 J. Liu, T. Fu, C. Liu, F. Wu and H. Wang, *Nanotechnology*, 2021, **32**, 355503.
47 J.-J. Max and C. Chapados, *J. Phys. Chem. A*, 2004, **108**, 3324–3337.
48 M. Avais and S. Chattopadhyay, *J. Mater. Chem. A*, 2022, **10**, 20090–20100.
49 C. Shen, J. Wang, Y. Cao and Y. Lu, *J. Mater. Chem. C*, 2015, **3**, 6668–6675.
50 B. Liu, B. Chu, Y.-L. Wang, L.-F. Hu, S. Hu and X.-H. Zhang, *Green Chem.*, 2021, **23**, 422–429.
51 S. Lu, L. Sui, J. Liu, S. Zhu, A. Chen, M. Jin and B. Yang, *Adv. Mat.*, 2017, **29**, 1603443.
52 S. Kumari and S. Chattopadhyay, *Mol. Syst. Des. Eng.*, 2024, **9**, 490–499.
53 M. Avais and S. Chattopadhyay, *J. Mater. Chem. A*, 2022, **10**, 20090–20100.
54 A. Desmecht, T. Steenhaut, F. Pennetreau, S. Hermans and O. Riant, *Chem. – Eur. J.*, 2018, **24**, 12992–13001.
55 L. Xia, B. Shentu and Z. Weng, *Polym. Compos.*, 2014, **35**, 627–635.
56 M. Golshan, B. Gheitarani, M. Salami-Kalajahi and M. S. Hosseini, *Sci. Rep.*, 2022, **12**, 15180.
57 A. Dashtdar, H. Yazadani-Ahmadabadi, A. Rezvani-Moghaddam, M. Salami-Kalajahi and U. Sundararaj, *Appl. Surf. Sci.*, 2024, **665**, 160286.
58 W. Yang, S. Wang, R. Li, J. Xu and W. Hao, *React. Funct. Polym.*, 2018, **133**, 57–65.
59 Q. Huang, J. Cheng, Y. Tang, Y. Wu, D. Xia, Y. Zheng and M. Guo, *Macromol. Rapid Commun.*, 2021, **42**, 2100174.
60 T. Zimmermann, J. Rietdorf, A. Girod, V. Georget and R. Pepperkok, *FEBS Lett.*, 2002, **531**, 245–249.
61 S. Chen, Y.-L. Yu and J.-H. Wang, *Anal. Chim. Acta*, 2018, **999**, 13–26.
62 O. M. K. Koç, A. Uzer and R. A. Apak, *ACS Appl. Mater. Interfaces*, 2023, **15**, 42066–42079.
63 S. Roth, P. Trinh and J. Wachtveitl, *Nanoscale*, 2021, **13**, 9808–9815.
64 S. Hussain, A. H. Malik, M. A. Afroz and P. K. Iyer, *Chem. Commun.*, 2015, **51**, 7207–7210.
65 H. W. Yang, P. Xu, B. Ding, Z. Y. Liu, X. J. Zhao and E. C. Yang, *Chem. – Eur. J.*, 2019, **2019**, 5077–5084.
66 A. Kathiravan, M. Narayanan, M. A. Jhonsi and V. Anbazhagan, *Spectrochim. Acta, Part A*, 2023, **303**, 123166.